Supplemental Material

Influence of ferroelectric order on the surface electronic structure of $BaTiO_3$ films studied by photoemission

Stefan Muff[1,2], Nicolas Pilet[2], Mauro Fanciulli[1,2], Andrew P. Weber[1,2], Christian Wessler[2], Zoran Ristić[2], Zhiming Wang[2,3], Nicholas C. Plumb[2], Milan Radović[2], and J. Hugo Dil[1,2]
[1] *Institut de Physique, École Polytechnique Fédérale de Lausanne, CH-1015 Lausanne, Switzerland*
[2] *Photon Science Department, Paul Scherrer Institut, CH-5232 Villigen, Switzerland*
[3] *Department of Quantum Matter Physics, University of Geneva, CH-1211 Geneva 4, Switzerland*
(Dated: June 17, 2018)

CONTENTS

I. TOPOGRAPHY OF THE $SrTiO_3$ AND $KTaO_3$ SUBSTRATES

The atomic force microscopy (AFM) topographies of $SrTiO_3$(001) (STO) and $KTaO_3$(001) (KTO) substrates as used for the growth of the BTO films of this study, are presented in Fig. S1. These data are taken with a different device than the PFM data in Fig.**??**. The STO substrate is etched to obtain a TiO_2 terminated surface. The etching procedure is described in the SOM of Plumb et al. [S1]. The measured AFM topography in Fig. S1(a) shows the presence of terraces with a width of approximately 210 nm. The KTO substrate is not etched and accordingly shows a mixed termination in the AFM data [Fig. S1(b)] in the form of higher (dark) patches. The observed terrace width is with approximately 120 nm roughly half the observed size of the STO substrate [Fig. S1(c)].

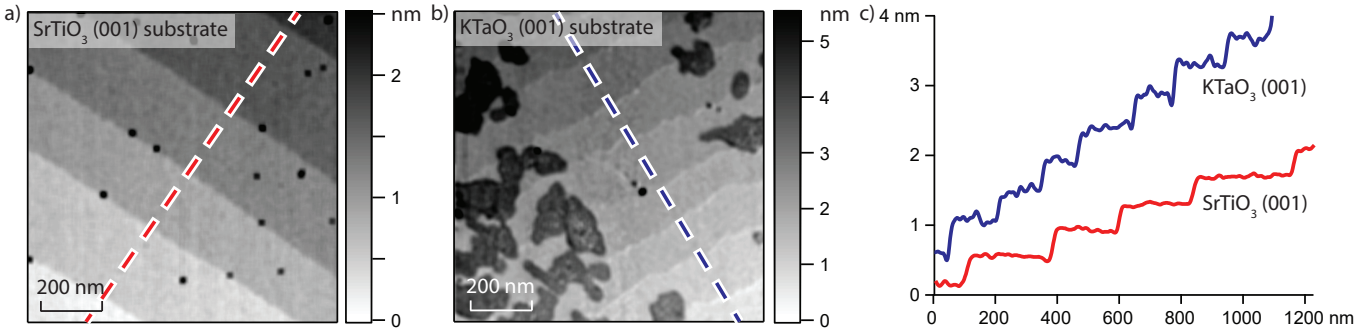

FIG. S1. (a) AFM topography of a $SrTiO_3$(001) substrate. (b) AFM topography of a $KTaO_3$(001) substrate. (c) Extracted line profiles along the dashed lines marked in (a,b) averaged over 25 nm width.

II. SUPPLEMENTAL ARPES MEASUREMENTS ON BTO

A. Photon Energy Dependency

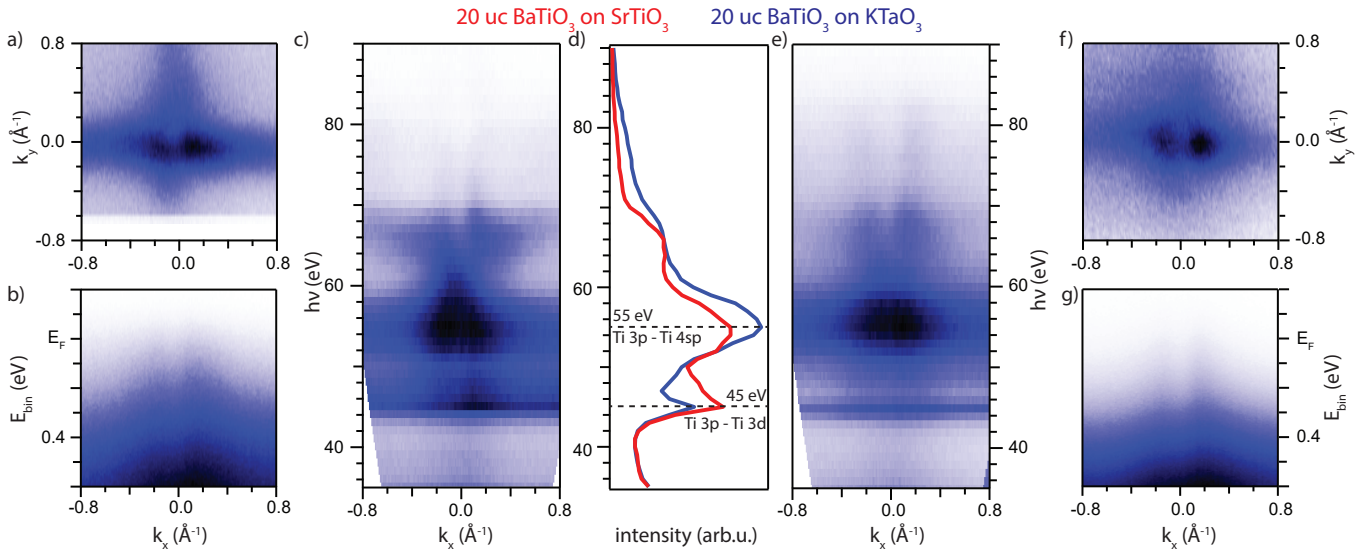

FIG. S2. ARPES data of 20 uc BTO grown on STO (a-c) and on KTO (e-g). (a,f) Fermi surface at $h\nu = 67$ eV and (b,g) Band dispersion in $\overline{\Gamma X}$-direction. (c,e) Photon energy scan from $h\nu = 35$ eV to 90 eV at the Fermi energy. (d) Integrated photoemission intensity over $k_x = \pm 0.6$ Å^{-1} at the Fermi energy for the sample grown on STO (red) and KTO (blue) substrate.

Fig. S2 depicts measured Fermi surfaces, band maps, and photon energy dependence of the two-dimensional states around $k_x = 0$ Å^{-1}, the $\overline{\Gamma_{00}}$ point. The measured intensity at the Fermi energy as a function of k_x and photon energy [Fig. S2(c,e)] shows bands, forming two parallel lines with photon energy close to $k_x = 0$ Å^{-1}, that corresponds to $\overline{\Gamma_{00}}$. The different photon energies give access to different k_z. Therefore the lack of dispersion of these two parallel bands with photon energy indicates their two-dimensional (or one-dimensional) nature. The observed intensity modulation with photonenergy is given by the excitation to different available final states as well as resonant enhancements. The photon energies of $h\nu = 45$ eV and $h\nu = 55$ eV [Fig. S2(d)] correspond to the energies of the Ti 3p - Ti 3d and Ti 3p - Ti 4sp resonance, respectively [S10, S11]. The Ti 3p - 3d resonance has a sharp Fano-like lineshape [S12] indicating a low dimensionality of the excited state [S11]; i.e. the Ti 3d states close to the Fermi level. On the other hand, the Ti 3p - Ti 4sp resonance is much broader implying that these states, hybridized with oxygen, are more delocalized along the z-direction [S11].

B. Light Polarizations

The Fermi surfaces and corresponding band structures for right- and left hand circularly polarized light as well as for s- and p-polarized linear light are depicted in Fig. S3 and Fig. S4. For these data, the analyzer entrance slit is aligned along the $\overline{\Gamma X}$-direction of the sample as in the main text. For s-polarized light the electric field of the synchrotron light is along the k_y-direction, for p-polarized light along the k_x-direction [see Fig. **??**(a)]. In the data in the vicinity $\overline{\Gamma_{00}}$ [Fig. S3] measured with a photon energy of $h\nu = 67$ eV no differences are noticeable for the two circular polarizations [Fig. S3(a,b)]. The band dispersion along the k_x-direction for circularly polarized light shows two features, connected to the in-gap state as discussed in the main text. Along k_y the band structure only hosts a single intensity feature at $k_y = 0$ Å^{-1}.

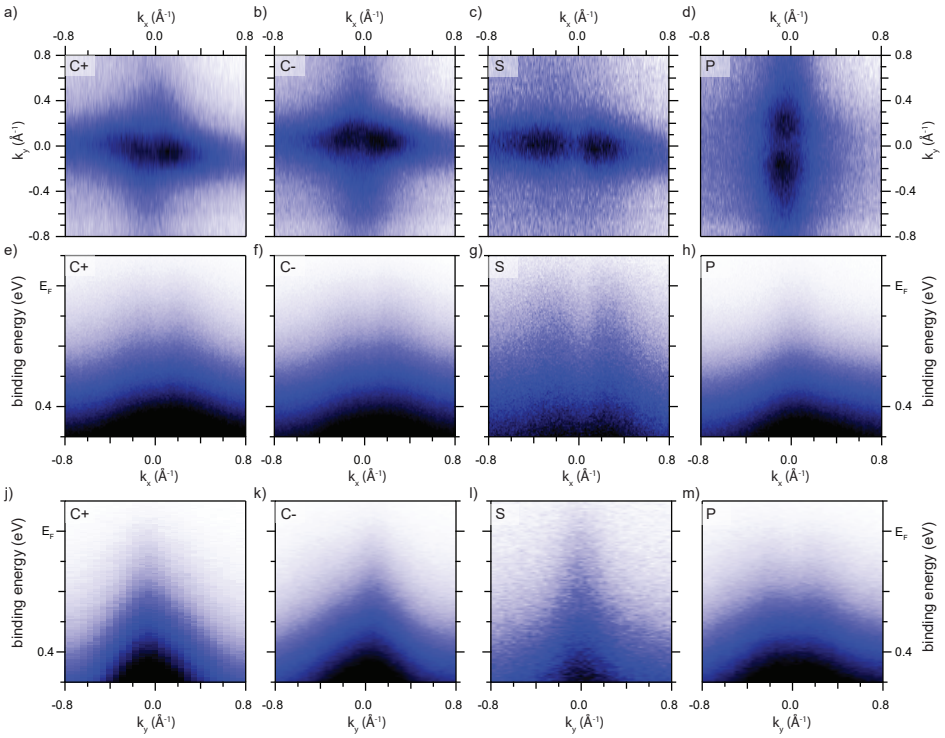

FIG. S3. ARPES data of 20 uc BTO on STO for different light polarizations measured with $h\nu = 67$ eV. (a-d) Fermi surfaces of the first Brillouin zone around $\overline{\Gamma_{00}}$ for (a) left- and (b) right-hand circularly polarized light and linear (c) s- and (d) p-polarized light. (e-h) Band dispersions along the k_x-direction for $k_y = 0$ Å^{-1} and (j-m) band dispersions along the k_y-direction ($k_x = 0$ Å^{-1}) for the four light polarizations.

For s-polarized light [Fig. S3(c)], the Fermi surface consist of two features elongated along the k_x-direction, separated by suppressed intensity at $k_x = 0$ Å^{-1}. Accordingly two features appear in the k_x dispersion, and the k_y dispersion only shows enhanced intensity around $k_y = 0$ Å^{-1}. The Fermi surface with p-polarized light [Fig. S3(d)] is similar to the one measured with s-polarized light but 90° rotated, with suppressed intensity along $k_y = 0$ Å^{-1}.

The suppressed intensity for $k_x = 0$ Å^{-1} with s-polarized light and for $k_y = 0$ Å^{-1} with p-polarized light is an indication for an xy-symmetry of the probed orbitals. In the case of the other known perovskites hosting a two-dimensional electron gas [S1, S13–S17], the two-dimensional states are attributed to the Ti $3d_{xy}$ orbitals and the three-dimensional bands, dispersing with photon energy, with the Ti $3d_{xz}$ and Ti $3d_{yz}$ orbitals. It seems likely for BTO to have a similar orbital ordering. However, due to the WSL of the states at the BTO surface, the orbital symmetries of the states present cannot be conclusively assigned.

The data in Fig. S4 of the Fermi surface at $\overline{\Gamma_{10}}$ for the different light polarizations are very similar to the data of $\overline{\Gamma_{00}}$ with respect to the light polarization effects. For right- as well as left-hand circularly polarized light [Fig. S4(a,b)] the intensity of the WSL along $\overline{\Gamma X}$ is visible. However, the intensity distribution along k_y around the Γ-point is inverted. For the linear polarized light only the WSL states in k_x-direction are visible for s-polarized light, while for p-polarized light only intensity elongated in k_y-direction are present. In contrast to the data taken at $\overline{\Gamma_{00}}$, the suppression of intensity at $k_x = 0$ Å^{-1} or $k_y = 0$ Å^{-1} for linear polarized light is absent due to the emission angle of $\overline{\Gamma_{10}}$ being far off

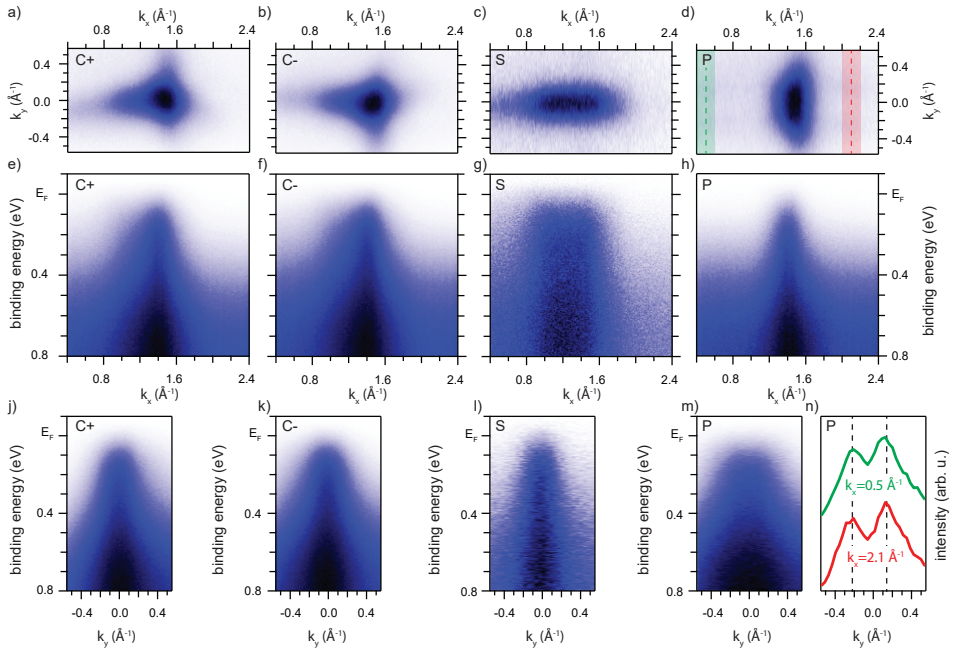

FIG. S4. Light polarization dependent ARPES of 20 uc BTO on STO measured with $h\nu = 80$ eV. (a-d) Fermi surfaces of the second Brillouin zone showing $\overline{\Gamma_{10}}$ for (a) C+, (b) C-, (c) s- and (d) p-polarized light. (e-h) Corresponding band dispersions along the k_x-direction for $k_y = 0$ Å^{-1} and (j-m) band dispersion along the k_y-direction at $k_x = 1.57$ Å^{-1} for the four light polarizations. (n) Momentum distribution curves taken at the Fermi energy along k_y for two fixed k_x integrated over 0.2 Å^{-1} as indicated in (d).

normal emission. The band dispersion along the k_y-direction for the four different light polarizations consist of a main feature around $\overline{\Gamma_{10}}$, dispersing from the in-gap state. The band dispersions for the circular polarized lights, show an asymmetry around $k_y = 0$ Å^{-1} corresponding with the Fermi surface. For s-polarized light the feature is narrow in the k_y-direction while for p-polarized light it is broad, opposite to the band dispersions along the k_x-direction.

Not only the intensity distribution around the $\overline{\Gamma}$-points, but also in between is strongly affected by the light polarization. A clear example of this is the data obtained with p-polarized light in Fig. S4(d) where at k_x values away from $\overline{\Gamma_{10}}$ two horizontal lines are visible around $k_y = \pm 0.2$ Å^{-1}. In the momentum distribution curves shown in Fig. S4(n) these lines along k_x are resolved as two peaks. Their origin can be understood by considering that with p-polarized light primarily the top and bottom part of the circular Fermi surface around the $\overline{\Gamma}$-point are probed [S17]. Due to Wannier-Stark localization in the domains oriented along the x-direction these parts of the Fermi surface are smeared out and form two lines along k_x.

III. FURTHER CHARACTERIZATION OF STO THIN FILMS

A. RHEED pattern and Oscillations

The growth process with pulsed laser deposition (PLD), was monitored by reflective high-energy electron diffraction (RHEED) patterns and oscillations. The RHEED pattern and oscillations of a film of 20 uc BTO grown on a STO substrate are depicted in Fig. S5(a,d). The RHEED pattern was obtained after the growth and indicates a crystalline two-dimensional surface. Each maxima of the RHEED oscillation corresponds to the formation of a complete BTO layer and therefore allows a precise thickness control of the film while growing. The RHEED pattern of the 3 uc [Fig. S5(b)] and 5 uc [Fig. S5(c)] film of STO deposited on a previously grown BTO film of 20 uc shows a good crystalline surface. By the help of the RHEED oscillations of the STO thin film growth [Fig. S5(e)], a precise termination of the growth process is possible at the oscillation maxima.

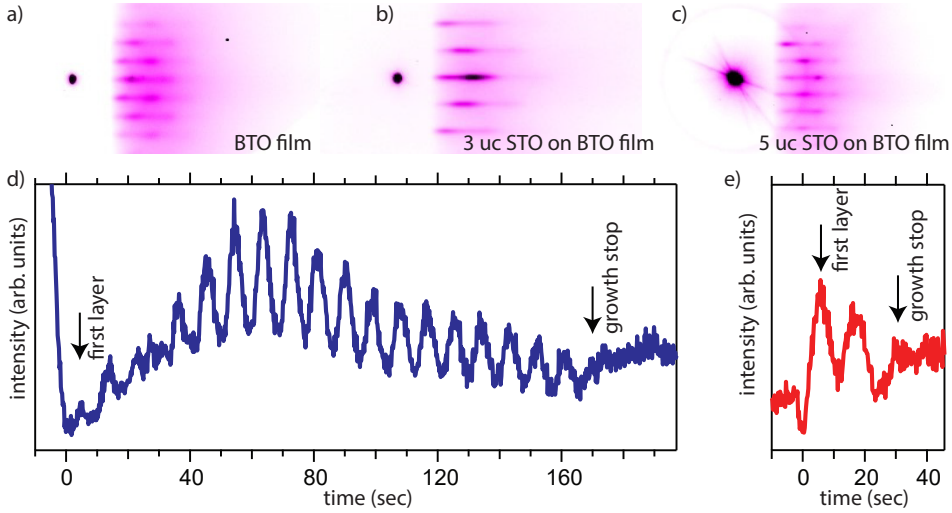

FIG. S5. (a) RHEED pattern of 20 uc BTO film grown on STO , (b) pattern of 3 uc STO grown on a BTO film and (c) pattern of 5 uc STO grown on a BTO film. (d) RHEED oscillations during the growth of the BTO film. (e) RHEED oscillations of 3 uc STO grown on a 20 uc STO film.

B. ARPES Measurements

In Fig. 3(a) of the main text a subsection of the Fermi surface for a 3 uc thick film of STO grown on a 20 uc film of BTO was shown. Although the WSL states are readily discernible their extension becomes more clearly visible in the large range Fermi surface map in Fig. S6(a).

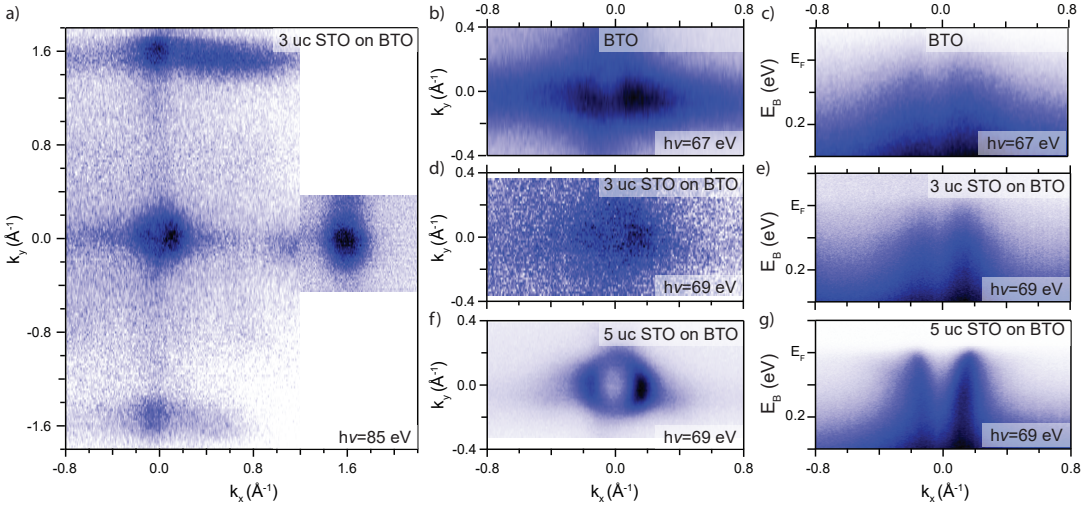

FIG. S6. (a) Fermi surface of 3 uc of STO on BTO obtained at $h\nu = 85$ eV. (b,d,f) Fermi surfaces around the surface Brillouin zone center for pure BTO, 3 uc, and 5 uc of STO on BTO at the indicated photon energies. (c,e,g) Band maps at $k_y = 0$ for pure BTO, 3 uc, and 5 uc of STO on BTO at the indicated photon energies.

In Fig S6(b-g) a comparison between pure BTO, 3 uc of STO on BTO, and 5 uc of STO on BTO is shown for a different photon energy as in Fig. 3 of the main text. Although the intensity ratio between the $3d_{xy}$ and $3d_{xz}$ (or $3d_{yz}$) bands has changed for the 5 uc data, the general features are independent of photon energy.

[S1] N. C. Plumb, M. Salluzzo, E. Razzoli, M. Månsson, M. Falub, J. Krempasky, C. E. Matt, J. Chang, M. Schulte, J. Braun, H. Ebert, J. Minár, B. Delley, K.-J. Zhou, T. Schmitt, M. Shi, J. Mesot, L. Patthey, and M. Radović, Phys. Rev. Lett. **113**, 086801 (2014).

[S2] R. Feynman, R. Leighton, and M. Sands, *Feynman Lectures on Physics: Volume 2* (Addison-Wesley, 1964).

[S3] P. Hofmann, *Solid State Physics - An Introduction* (Wiley VCH, 2014) online notes.

[S4] W. J. Merz, Phys. Rev. **91**, 513 (1953).

[S5] T. Hayashi, N. Oji, and H. Maiwa, Japanese journal of applied physics **33**, 5277 (1994).

[S6] O. Trithaveesak, J. Schubert, and C. Buchal, Journal of applied Physics **98**, 114101 (2005).

[S7] E. Mendez, F. Agullo-Rueda, and J. Hong, Physical review letters **60**, 2426 (1988).

[S8] P. Voisin, J. Bleuse, C. Bouche, S. Gaillard, C. Alibert, and A. Regreny, Physical review letters **61**, 1639 (1988).

[S9] M. P. Marder, *Condensed Matter Physics, 2nd Edition* (Wiley, 2010).

[S10] K. E. Smith and V. E. Henrich, Physical Review B **38**, 9571 (1988).

[S11] J. Tao, T. Luttrell, and M. Batzill, Nature chemistry **3**, 296 (2011).

[S12] U. Fano, Physical Review **124**, 1866 (1961).

[S13] A. F. Santander-Syro, O. Copie, T. Kondo, F. Fortuna, S. Pailhès, R. Weht, X. G. Qiu, F. Bertran, A. Nicolaou, A. Taleb-Ibrahimi, P. L. Fèvre, G. Herranz, M. Bibes, N. Reyren, Y. Apertet, P. Lecoeur, A. Barthélémy, and M. J. Rozenberg, Nature **469**, 189 (2011).

[S14] W. Meevasana, P. D. C. King, R. H. He, S.-K. Mo, M. Hashimoto, A. Tamai, P. Songsiriritthigul, F. Baumberger, and Z.-X. Shen, Nat Mater **10**, 114 (2011).

[S15] P. D. C. King, R. H. He, T. Eknapakul, P. Buaphet, S. K. Mo, Y. Kaneko, S. Harashima, Y. Hikita, M. S. Bahramy, C. Bell, Z. Hussain, Y. Tokura, Z. X. Shen, H. Y. Hwang, F. Baumberger, and W. Meevasana, Physical Review Letters **108**, 117602 (2012).

[S16] A. F. Santander-Syro, C. Bareille, F. Fortuna, O. Copie, M. Gabay, F. Bertran, A. Taleb-Ibrahimi, P. Le Fèvre, G. Herranz, N. Reyren, M. Bibes, A. Barthélémy, P. Lecoeur, J. Guevara, and M. J. Rozenberg, Phys. Rev. B **86**, 121107 (2012).

[S17] S. Muff, M. Fanciulli, A. P. Weber, N. Pilet, Z. Ristic, Z. Wang, N. C. Plumb, M. Radovic, and J. H. Dil, Applied Surface Science **432**, 41 (2017).